nature catalysis

SUPPLEMENTARY INFORMATION

https://doi.org/10.1038/s41929-019-0347-y

In the format provided by the authors and unedited.

Efficient reductive desymmetrization of bulky 1,3-cyclodiketones enabled by structure-guided directed evolution of a carbonyl reductase

Xi Chen[1,5], Hongliu Zhang[1,5], Miguel A. Maria-Solano[2], Weidong Liu[1], Juan Li[1,3], Jinhui Feng[1], Xiangtao Liu[1], Sílvia Osuna[2,4]*, Rey-Ting Guo[1], Qiaqing Wu[1]*, Dunming Zhu[1,3]* and Yanhe Ma[1]

[1]National Engineering Laboratory for Industrial Enzymes and Tianjin Engineering Research Center of Biocatalytic Technology, Tianjin Institute of Industrial Biotechnology, Chinese Academy of Sciences, Tianjin, China. [2]CompBioLab group, Institut de Química Computacional i Catàlisi, Department of Chemistry, University of Girona, Girona, Spain. [3]University of the Chinese Academy of Sciences, Beijing, China. [4]ICREA, Barcelona, Spain. [5]These authors contributed equally: Xi Chen and Hongliu Zhang. *e-mail: silvia.osuna@udg.edu; wu_qq@tib.cas.cn; zhu_dm@tib.cas.cn

Supplementary information for:

Efficient Reductive Desymmetrization of Bulky 1,3-Cyclodiketones Enabled by Structure-Guided Directed Evolution of a Carbonyl Reductase

Xi Chen[1,5], Hongliu Zhang[1,5], Miguel A. Maria Solano[2], Weidong Liu[1], Juan Li[1,4], Jinhui Feng[1], Xiangtao Liu[1], Sílvia Osuna[2,3*], Rey-Ting Guo[1], Qiaqing Wu[1,*], Dunming Zhu[1,4*] and Yanhe Ma[1]

[1]National Engineering Laboratory for Industrial Enzymes and Tianjin Engineering Research Center of Biocatalytic Technology, Tianjin Institute of Industrial Biotechnology, Chinese Academy of Sciences, Tianjin, 300308, China;

[2]CompBioLab group, Institute of Computational Chemistry and Catalysis, Department of Chemistry, University of Girona, Girona, Spain;

[3]ICREA, Passeig Lluís Companys 23, 08010 Barcelona, Spain;

[4]University of Chinese Academy of Sciences, Shijingshan District, Beijing 100049, China.

[5]These authors contributed equally: Xi Chen and Hongliu Zhang

E-mail: zhu_dm@tib.cas.cn, silviaosu@gmail.com, wu_qq@tib.cas.cn

Supplementary Methods

Characterisation of 2,2-disubstituted 1,3-cyclopentanediones[1]

2-ethyl-2-benzylcyclopentane-1,3-dione (**1b**) (86% yield). ^{1}H NMR (600 MHz, $CDCl_3$): δ 7.23-7.18 (m, 3H), 6.98-7.03 (m, 2H), 2.93 (s, 2H), 2.44-2.59 (m, 2H,), 195-2.10 (m, 2H), 1.17 (s, 3H).

2-methyl-2-benzylcyclopentane-1,3-dione (**3a**, 69% yield). ^{1}H NMR (600 MHz, $CDCl_3$):

δ 7.16-7.24 (m, 3H), 6.99-7.06 (m, 2H), 2.94 (s, 2H), 2.39-2.49 (m, 2H), 1.95-2.05 (m, 2H), 1.82 (q, *J* = 4.2, 10.4 Hz, 2H), 0.79 (t, *J* = 7.8 Hz 3H).

2-methyl-2-(2-methylbenzyl)cyclopentane-1,3-dione (**3b**, 76% yield). ^{1}H NMR (600 MHz, $CDCl_3$): δ 7.09-7.12 (m, 2H), 7.04-7.06 (m, 1H), 6.95-6.97 (m, 1H), 3.02 (s, 2H), 2.48-2.87 (m, 2H), 2.25 (s, 2H), 2.09-2.18 (m, 2H), 1.17 (s, 3H).

2-methyl-2-(3-methylbenzyl)cyclopentane-1,3-dione (**3c**, 72% yield). ^{1}H NMR (600 MHz, $CDCl_3$): δ 7.10-7.14 (m, 1H), 6.99-7.04 (m, 1H), 6.81-6.89 (m, 2H), 2.93 (s, 2H), 2.41-2.51 (m, 2H), 2.20 (s, 3H), 1.96-2.05 (m, 2H), 1.12 (s, 2H).

2-methyl-2-(4-methylbenzyl)cyclopentane-1,3-dione (**3d**, 83% yield**)**. ^{1}H NMR (600 MHz, $CDCl_3$): δ 6.95 (2H, d, *J* = 4.8 Hz), 6.95 (2H, d, *J* = 4.2 Hz), 2.84 (s, 2H), 2.48-2.62 (m, 2H), 2.29 (s, 3H), 2.00-2.15 (m, 2H), 1.21 (s, 3H).

2-methyl-2-(2-chlorobenzyl)cyclopentane-1,3-dione (**3e**, 65% yield). ^{1}H NMR (600 MHz, $CDCl_3$): δ 7.33-7.37 (m, 1H), 7.18-7.22 (m, 2H), 7.11-7.15 (m, 1H), 3.13 (s, 2H), 2.60-2.69 (m, 2H), 2.52-2.59 (m, 2H), 1.21 (s, 3H).

2-methyl-2-(3-chlorobenzyl)cyclopentane-1,3-dione (**3f**, 72% yield). ^{1}H NMR (600 MHz, $CDCl_3$): δ 7.07-7.21 (m, 1H), 7.01-7.06 (m, 2H), 6.86-6.96 (m, 1H), 2.92 (s, 2H), 2.51-2.70 (m, 2H), 2.06-2.23 (m, 2H), 1.19 (s, 3H).

2-methyl-2-(4-chlorobenzyl)cyclopentane-1,3-dione (**3g**, 79% yield). ^{1}H NMR (600 MHz, $CDCl_3$): δ 7.17-7.27 (m, 2H), 6.95-7.00 (m, 2H), 2.92 (s, 2H), 2.54-2.68 (m, 2H), 2.05-2.20 (m, 2H), 1.19 (s, 3H).

2-methyl-2-(3-bromobenzyl)cyclopentane-1,3-dione (**3h**, 73% yield). ^{1}H NMR (600 MHz, $CDCl_3$): δ 7.30-7.36 (m, 1H), 7.01-7.18 (m, 2H), 6.92-7.02 (m, 1H), 2.91 (s, 2H), 2.53-2.70 (m, 2H), 2.06-2.23 (m, 2H), 1.20 (s, 3H).

2-methyl-2-(4-bromobenzyl)cyclopentane-1,3-dione (**3i**, 81% yield). ^{1}H NMR (600 MHz, $CDCl_3$): δ 7.27-7.36 (m, 2H), 6.88-6.93 (m, 2H), 2.89 (s, 2H), 2.53-2.68 (m, 2H), 2.06-2.19 (m, 2H), 1.18 (s, 3H).

2-methyl-2-(naphthalen-2-ylmethyl)cyclopentane-1,3-dione (**3j**, 69% yield). ^{1}H NMR (600 MHz, $CDCl_3$): δ 7.79-7.73 (m, 2H), 7.69-7.73 (m, 1H), 7.51 (s, 1H), 7.41-7.48 (m, 2H), 7.13-7.19 (m, 1H), 3.13 (s, 2H), 2.48-2.58 (m, 2H), 1.96-2.06 (m, 2H), 1.26 (s, 3H).

2-allyl-2-methylcyclopentane-1,3-dione (**3k**, 59% yield). ^{1}H NMR (600 MHz, $CDCl_3$): δ 5.55-5.64 (m, 1H), 5.04-5.10 (m, 2H), 2.64-2.80 (m, 4H), 2.33-2.38 (m, 2H), 1.12 (s, 3H).

2-methyl-2-(prop-2-yn-1-yl)cyclopentane-1,3-dione **3l** (62% yield). ^{1}H NMR (600 MHz, $CDCl_3$): δ 2.71-2.89 (m, 4H), 2.43 (d, *J* = 1.2 Hz, 2H), 1.95 (t, *J* = 2.4, 3.0 Hz, 2H), 1.10 (s, 3H).

Characterisation of 2,2-disubstituted 3-hydroxycyclo-1-pentanones

(13*R*,17*S*)-ethyl secol (**2a**, 94% yield). ^{1}H NMR (600 MHz, $CDCl_3$): δ 7.10 (d, *J* = 6.0 Hz, 1H), 6.68-6.74 (m, 3H), 5.71 (t, *J* = 18 Hz, 1H), 4.22 (t, *J* = 18 Hz, 1H), 3.77 (s, 3H), 2.64-2.70 (m, 2H), 2.41-2.49 (m, 1H); 2.31-2.38 (m, 2H), 2.13-2.29 (m, 4H), 1.84-1.95 (m, 1H), 1.62-1.74 (m, 3H), 1.51-1.60 (m, 1H), 0.93 (t, *J* = 5.6 Hz, 3H).

(2*R*,3*S*)-2-benzyl-3-hydroxy-2-ethylcyclopentanone (**2b**, 82% yield). ^{1}H NMR (600 MHz, $CDCl_3$): δ 7.24-7.30 (m, 2H), 7.20-7.23 (m, 1H), 7.12-7.15 (m, 2H), 4.23 (t, *J* = 4.8 Hz, 1H), 2.92(d, *J* = 12.6 Hz, 1H), 2.75 (d, *J* = 12.6 Hz, 1H), 2.37-2.45 (m, 1H), 2.03-2.10 (m, 1H), 1.94-2.02 (m, 1H), 1.78-1.86 (m, 1H), 1.62-1.70 (m, 1H), 1.52-1.61 (m, 1H), 0.99 (t, *J* = 5.4 Hz, 3H). ^{13}C NMR (125 MHz, $CDCl_3$): δ 219.1, 137.6, 139.9, 128.5, 126.6, 74.5, 57.1, 37.9, 35.6, 27.8, 22.0, 8.2. HRMS (ES^+) calcd for $C_{14}H_{18}O_2$ (M+Na): 241.1204, found: 241.1213. $[\alpha]_D^{25}$ -19.1 (c 0.5, CH_3CH_2OH).

(2*R*,3*S*)-2-benzyl-3-hydroxy-2-methylcyclopentanone (**4a**, 82% yield). ^{1}H NMR (600 MHz, $CDCl_3$): δ 7.21-7.31 (m, 4H), 7.14 (m, 1H), 4.20 (t, *J* = 4.8 Hz, 1H), 2.87 (d, *J* = 12.6 Hz, 1H), 2.70 (d, *J* = 12.6 Hz, 1H), 2.42-2.49 (m, 1H), 2.11-2.18 (m, 1H), 1.99-2.08 (m, 1H), 1.75-1.85 (m, 1H), 1.03 (s, 3H). ^{13}C NMR (125 MHz, $CDCl_3$): δ 220.2, 137.5, 130.2, 128.7, 126.9, 74.5, 54.2, 41.3, 35.5, 27.5, 16.1. HRMS (ES^+) calcd for $C_{13}H_{16}O_2$ (M+Na): 227.1048, found: 227.1096. $[\alpha]_D^{25}$ -43.6 (c 0.5, CH_3CH_2OH).

(2*R*,3*S*)-3-hydroxy-2-methyl-2-(2-methylbenzyl)cyclopentanone (**4b**, 85% yield). ^{1}H NMR (600 MHz, $CDCl_3$): δ 7.03-7.14 (m, 4H), 4.12 (t, *J* = 2.4 Hz, 1H), 2.77-2.97 (m, 2H), 2.42 (m, 1H), 2.33 (3H, s), 2.12 (m, 1H), 1.97 (m, 1H), 1.74 (m, 1H), 1.02 (s, 3H). ^{13}C NMR (125 MHz, $CDCl_3$): δ 220.1, 137.4, 136.2, 130.6, 126.9, 126.2, 74.5, 54.8, 37.4, 36.0, 27.8, 20.3, 16.6. HRMS (ES^+) calcd for $C_{14}H_{18}O_2$ (M+Na): 241.1204, found: 241.1252. $[\alpha]_D^{25}$ -75.2 (c 0.5, CH_3CH_2OH).

(2*R*,3*S*)-3-hydroxy-2-methyl-2-(3-methylbenzyl)cyclopentanone (**4c**, 88% yield). ^{1}H NMR (600 MHz, $CDCl_3$): δ 6.89-7.19 (m, 4H), 4.12 (t, *J* = 2.4 Hz, 1H), 2.80 (d, *J* = 12 Hz, 1H,), 2.63 (d, *J* = 12 Hz, 1H), 2.42 (m, 1H), 2.29 (s, 3H), 2.11 (m, 1H), 2.01 (m, 1H), 1.76 (m, 1H), 1.01 (s, 3H). ^{13}C NMR (125 MHz, $CDCl_3$): δ 220.3, 138.3, 137.4, 131.0, 128.6,

127.7, 127.2, 74.5, 54.2, 41.3, 35.5, 27.5, 21.6, 16.2. HRMS (ES^+) calcd for $C_{14}H_{18}O_2$ (M+Na): 241.1204, found: 241.1240. $[\alpha]_D^{25}$ -61.1 (c 0.5, CH_3CH_2OH).

(2*R*,3*S*)-3-hydroxy-2-methyl-2-(4-methylbenzyl)cyclopentanone (**4d**, 88% yield). ^1H NMR (600 MHz, $CDCl_3$): δ 7.06 (d, *J* = 3.6 Hz, 2H), 6.99 (d, *J* = 3.6 Hz, 2H), 4.18 (t, *J* = 1.2, 12 Hz, 1H), 2.80 (d, *J* = 6.0 Hz, 1H), 2.63 (d, *J* = 12 Hz, 1H), 2.42 (m, 1H), 2.29 (s, 3H), 2.11 (m, 1H), 2.01 (m, 1H), 1.76 (m, 1H), 0.99 (s, 3H). ^{13}C NMR (125 MHz, $CDCl_3$): δ 220.3, 136.5, 134.3, 130.1, 129.4, 74.5, 54.3, 40.9, 35.5, 27.5, 21.2, 16.1. HRMS (ES^+) calcd for $C_{14}H_{18}O_2$ (M+Na): 241.1204, found: 241.1241. $[\alpha]_D^{25}$ -65.2 (c 0.5, CH_3CH_2OH).

(2*R*,3*S*)-3-hydroxy-2-methyl-2-(2-chlorobenzyl)cyclopentanone (**4e**, 89% yield). ^1H NMR (600 MHz, $CDCl_3$): δ 7.34-7.39 (m, 1H), 7.15-7.22 (m, 3H), 4.13 (m, 1H), 3.00-3.11 (m, 2H), 2.43-2.49 (m, 1H), 2.12-2.19 (m, 1H), 1.91-1.99 (m, 1H), 1.79-1.88 (m, 1H), 1.09 (s, 3H). ^{13}C NMR (125 MHz, $CDCl_3$): δ 219.6, 135.7, 135.0, 132.6, 129.6, 128.4, 127.3, 73.9, 55.1, 37.2, 36.0, 26.9, 16.9. HRMS (ES^+) calcd for $C_{14}H_{18}ClO_2$ (M+Na): 261.0658, found: 261.0674. $[\alpha]_D^{25}$ -26.5 (c 0.5, CH_3CH_2OH).

(2*R*,3*S*)-3-hydroxy-2-methyl-2-(3-chlorobenzyl)cyclopentanone (**4f**, 92% yield). ^1H NMR (600 MHz, $CDCl_3$): δ 7.03-7.22 (m, 4H), 4.12 (t, *J* = 6.0 Hz, 1H), 2.86 (d, *J* = 12.6 Hz, 1H), 2.63 (d, *J* = 12.6 Hz, 1H), 2.45 (m, 1H), 2.13 (m, 1H), 2.00 (m, 1H), 1.80 (m, 1H), 1.01 (s, 3H). ^{13}C NMR (125 MHz, $CDCl_3$): δ 219.5, 139.6, 134.4, 130.3, 129.8, 128.5, 127.1, 74.0, 54.3, 40.7, 35.6, 27.7, 16.3. HRMS (ES^+) calcd for $C_{14}H_{18}ClO_2$ (M+Na): 261.0658, found: 261.0654. $[\alpha]_D^{25}$ -54.7 (c 0.5, CH_3CH_2OH).

(2*R*,3*S*)-3-hydroxy-2-methyl-2-(4-chlorobenzyl)cyclopentanone (**4g**, 93% yield). ^1H NMR (600 MHz, $CDCl_3$): δ 7.21 (d, *J* = 3.6 Hz, 2H), 7.03 (d, *J* = 3.6 Hz, 2H), 4.10 (m, 1H), 2.86 (d, *J* = 12.6 Hz, 1H), 2.62 (d, *J* = 12.6 Hz, 1H), 2.38-2.49 (m, 1H), 2.06-2.17 (m, 1H), 1.92-2.01 (m, 1H), 1.72-1.83 (m, 1H), 0.99 (s, 3H). ^{13}C NMR (125 MHz, $CDCl_3$): δ 219.7, 136.0, 132.8, 131.6, 128.7, 74.0, 54.3, 40.4, 35.6, 27.7, 16.3. HRMS (ES^+) calcd for $C_{14}H_{18}ClO_2$ (M+Na): 261.0658, found: 261.0646. $[\alpha]_D^{25}$ -46.4 (c 0.5, CH_3CH_2OH).

(2*R*,3*S*)-3-hydroxy-2-methyl-2-(3-bromobenzyl)cyclopentanone (**4h**, 93% yield). ^1H NMR (600 MHz, $CDCl_3$): δ 6.98-7.34 (4H), 4.10 (1H, t, *J* = 6.0 Hz), 2.83 (d, *J* = 12.6 Hz, 1H), 2.59 (d, *J* = 12.6 Hz, 1H), 2.41 (m, 1H), 2.11 (m, 1H), 1.96 (m, 1H), 1.76 (m, 1H), 0.99 (s, 3H). ^{13}C NMR (125 MHz, $CDCl_3$): δ 219.6, 139.9, 133.2, 130.1, 130.0, 128.9, 122.6, 74.0, 54.3, 40.6, 35.7, 27.7, 16.3. HRMS (ES^+) calcd for $C_{13}H_{15}Br$ (M+Na):

305.0153, found: 305.0133. $[\alpha]_D^{25}$ -34.0 (c 0.5, CH_3CH_2OH).

(2*R*,3*S*)-3-hydroxy-2-methyl-2-(4-bromobenzyl)cyclopentanone (**4i**, 94% yield). ^{1}H NMR (600 MHz, $CDCl_3$): δ 7.36 (d, *J* = 3.6 Hz, 2H), 6.99 (d, *J* = 3.6 Hz, 2H,), 4.10 (1H, t, *J* = 1.2, 6.0 Hz), 2.84 (d, *J* = 12.6 Hz, 1H), 2.60 (d, *J* = 12.6 Hz, 1H), 2.42 (m, 1H), 2.11 (m, 1H), 1.96 (m, 1H), 1.77 (m, 1H), 0.99 (s, 3H). ^{13}C NMR (125 MHz, $CDCl_3$): δ 219.7, 136.5, 132.0, 131.7, 120.9, 74.0, 54.3, 40.4, 35.7, 27.5, 16.3. HRMS (ES^+) calcd for $C_{13}H_{15}Br$ (M+Na): 305.0153, found: 305.0137. $[\alpha]_D^{25}$ -46.0 (c 0.5, CH_3CH_2OH).

(2*R*,3*S*)-3-hydroxy-2-methyl-2-(naphthalen-2-ylmethyl)cyclopentanone (**4j**, 93% yield). ^{1}H NMR (600 MHz, $CDCl_3$): δ 7.71-7.83 (m, 3H), 7.60 (s, 1H), 7.40-7.47 (m, 2H), 7.21 (d, *J* = 3.6 Hz, 1H), 4.24 (t, *J* =6.0 Hz, 1H), 3.08 (d, *J* = 12.6 Hz, 1H), 2.85 (d, *J* = 12.6 Hz, 1H), 2.42-2.49 (m, 1H), 2.08-2.16 (m, 1H), 1.95-2.03 (m, 1H), 1.74-1.84 (m, 1H), 1.09 (s, 3H). ^{13}C NMR (125 MHz, $CDCl_3$): δ 219.7, 136.5, 132.0, 131.7, 120.9, 74.0, 54.3, 40.4, 35.7, 27.5, 16.3. HRMS (ES^+) calcd for $C_{17}H_{18}O_2$ (M+Na): 277.1204, found: 277.1210. $[\alpha]_D^{25}$ -54.9 (c 0.5, CH_3CH_2OH).

(2*R*,3*S*)-2-allyl-3-hydroxy-2-methylcyclopentanone (**4k**, 79% yield). ^{1}H NMR (600 MHz, $CDCl_3$): δ 5.69-5.78 (m, 1H), 5.05-5.13 (m, 2H), 4.20 (t, *J* =6.0 Hz, 1H), 2.42-2.49 (m, 1H), 2.20-2.27 (m, 1H), 2.11-2.19 (m, 4H), 1.81-1.88 (m, 1H), 1.09 (s, 3H). HRMS (ES^+) calcd for $C_9H_{14}O_2$ (M+Na): 177.0891, found: 177.0884. $[\alpha]_D^{25}$ -29.1 (c 0.5, CH_3CH_2OH).

(2*R*,3*S*)-3-hydroxy-2-methyl-2-(prop-2-yn-1-yl)cyclopentanone (**4l**, 75% yield). ^{1}H NMR (600 MHz, $CDCl_3$): δ 2.40-2.44 (m, 1H), 2.47-2.54 (m, 2H), 7.25-7.28 (m, 1H), 2.13-2.42 (m, 5H), 1.82-1.91 (m, 1H), 1.07 (t, *J* = 5.4 Hz, 3H). ^{13}C NMR (125 MHz, $CDCl_3$): δ 218.6, 80.8, 75.5, 71.3, 51.9, 35.1, 27.3, 25.1, 15.2. HRMS (ES^+) calcd for $C_9H_{12}O_2$ (M+Na): 175.0735, found: 175.0723. $[\alpha]_D^{25}$ -70.8 (c 0.5, CH_3CH_2OH).

Supplementary Tables

Supplementary Table 1 Reduction of ethyl secodione with carbonyl reductases.

Enzyems	Conversion %	Ratio of mono-carbonyl reduction products % [a]			
		(13*R*, 17*R*)	(13*S*, 17*S*)	(13*S*, 17*R*)	(13*R*, 17*S*)
KERD-Pglu[2]	< 1	-	-	-	-
SSADH[3]	< 1	-	-	-	-
ZsADH[4]	2	33.6	42.5	-	23.9
Ymr226c[5]	3	> 99	-	-	-
TbADH[6]	5	0.6	-	-	99.4
Chkred12	8	89.2	10.8	-	-
H2[7]	10	56.2	-	-	43.8
Gre 2[8]	13	> 99	-	-	-
chkredF205A[9]	17	9.8	71.7	18.5	-
PFADH[10]	24	9.1	8.0	-	82.9
Yil124w[11]	60	52.4	1.2	-	46.4
LKADH[12]	63	33.7	50.1	16.2	-
ADH-A[13]	77	48.8	7.3	3.0	40.9
SSCR[14]	82	7.6	87.5	4.9	-
RasADH[15]	93	66.8	3.3	19.7	10.2
SSCR M242F/Q245T[b]	95	43.6	49.3	7.1	-

[a] The ratio of ketol products among all the four ketol products; [b] Preserved in our laboratory.

Supplementary Table 2 Data collection and refinement statistics of crystals.

	RasADH 3B3/I91V	RasADH F12
Data collection		
Space group	*$P6_1$*	*$P3_22_1$*
Unit-cell		
***a, b, c* [Å]**	69.08, 69.07, 388.99	118.69, 118.69, 73.01
***α /β /γ* (°)**	90.00/90.00/120.00	90.00/90.00/120.00
Resolution (Å)	25-1.78 (1.84-1.78)	25-1.80 (1.86-1.80)
Unique reflections	99773 (9987)	55225 (5156)
Redundancy	9.0 (9.3)	10.2 (8.6)
Completeness (%)	99.9 (100.0)	99.4 (93.6)
Average I/σ(I)	41.2 (3.56)	31.6 (2.79)
CC 1/2*	0.979 (0.862)	0.986 (0.947)
Refinement		
No. of reflections	99646 (9774)	55003 (5219)
R_{work} (95% data)	0.184 (0.260)	0.172 (0.212)
R_{free} (5% data)	0.214 (0.290)	0.213 (0.254)
Rmsd bonds (Å)	0.004	0.014
Rmsd angles (°)	0.943	1.356
Dihedral angles		
Most favored (%)	91.3	92.3
Allowed (%)	8.7	7.7
Disallowed (%)	0.0	0.0
no. of non-H atoms / average B [$Å^2$]		
Protein	7204/31.11	3651/26.98
Water	730/39.59	316/35.26
Ligand	190/61.18	119/40.33
PDB ID code	6IHI	6IHH

Values in parentheses are for the outermost resolution shells. *CC(1/2) = percentage of correlation between intensities from random half-datasets. Karplus & Diederichs (2012), Science 336, 1030-33

Supplementary Table 3 List of Primers.

Protein	Primers(5'-3')
L201 Forward	GAAGCTGACGAA**NNK**CGTGCTAAATTCGCTGCTG
L201 Reverse	GAATTTAGCACG**MNN**TTCGTCAGCTTCTTCCTG
F205 Forward	CTGCGTGCTAAA**NNK**GCTGCTGCTACCCCGCTG
F205 Reverse	GGTAGCAGCAGC**MNN**TTTAGCACGCAGTTCGTC
I187/I188 Forward	CTATCGACACCCCG**NDTNDT**GAAAACCAGGTTTCTACC
I187/I188 Reverse	GAAACCTGGTTTTC**AHNAHN**CGGGGTGTCGATAGCACC
I91/Q93 Forward	CTAACTCTGGTGCT**NDT**GAA**NDT**AAAACCCTGGAAGAAATC
I91/Q93 Reverse	CTTCCAGGGTTTT**AHN**TTC**AHN**AGCACCAGAGTTAGCGAAC
L144 Forward	GGTGTTCTGGGT**NNK**CAGGCTCACGACACCTAC
L144 Reverse	GTCGTGAGCCTG**MNN**ACCCAGAACACCAGCAAC
H147 Forward	GGTCTGCAGGCT**NNK**GACACCTACTCTGCTGC
H147 Reverse	CAGAGTAGGTGTC**MNN**AGCCTGCAGACCCAGAAC
Y150 Forward	GGCTCACGACACC**NNK**TCTGCTGCTAAAGCTGCTG
Y150 Reverse	CTTTAGCAGCAGA**MNN**GGTGTCGTGAGCCTGCAGACC
Q191 Forward	CGAGTCTTGAAAAC**NNK**GTTTCTACCCAGGAAG
Q191 Reverse	CTGGGTAGAAAC**MNN**GTTTTCAAGACTCGGGGTG
G89 Forward	GTTCGCTAACTCT**NNK**GCTGTTGAACAGAAAACCC
G89 Reverse	CTGTTCAACAGC**MNN**AGAGTTAGCGAACAGAAC
P101 Forward	GAAGAAATCACC**NNK**GAACACTACGACCGTACC
P101 Reverse	GGTCGTAGTGTTC**MNN**GGTGATTTCTTCCAGGG
N190 Forward	CCCCGAGTCTTGAA**NNK**CAGGTTTCTACCCAGGAAG
N190 Reverse	CTGGGTAGAAACCTG**MNN**TTCAAGACTCGGGGTGTCG
P180 Forward	GTTAACGCTGTTTCT**NNK**GGTGCTATCGACACCCCGAG
P180 Reverse	GTGTCGATAGCACC**MNN**AGAAACAGCGTTAACACGG
K154 Forward	CTACTCTGCTGCT**NNK**GCTGCTGTTCGTTCTCTG
K154 Reverse	CGAACAGCAGC**MNN**AGCAGCAGAGTAGGTGTCG
N111 Forward	CCTTCGACGTT**NNK**GTTCGTGGTCTGATCTTCAC
N111 Reverse	CAGACCACGAAC**MNN**AACGTCGAAGGTACGGTCG

Supplementary Table 4 The reduction of bulky diaryl ketones catalyzed by wild-type RasADH and mutant F12[a].

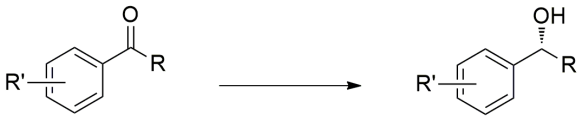

R′, R group	RasADH WT		RasADH F12	
	Specific activity (U/mg)	ee %	Specific activity (U/mg)	ee %
H, *o*-CH_3 phenyl (**5a**)	0.005	78 (*S*)	0.018	96 (*S*)
H, *p*-CH_3 phenyl (**5b**)	0.009	63 (*S*)	0.029	95 (*S*)
H, *o*-Cl phenyl (**5c**)	0.023	>99 (*S*)	0.047	>99 (*S*)
H, *p*-Cl phenyl (**5d**)	0.018	38 (*S*)	0.063	93 (*S*)
H, *p*-F phenyl (**5e**)	0.015	17 (*S*)	0.033	77 (*S*)
H, *p*-OCH_3 phenyl (**5f**)	0.005	79 (*S*)	0.018	97 (*S*)
H, 2-pyridyl (**5g**)	0.015	67 (*S*)	0.256	98 (*S*)
4′-Cl, 2-pyridyl (**5h**)	0.091	58 (*S*)	2.449	93 (*S*)

[a] The specific activity and the ee values were measured as described in the Supplementary Methods.

Supplementary Figures

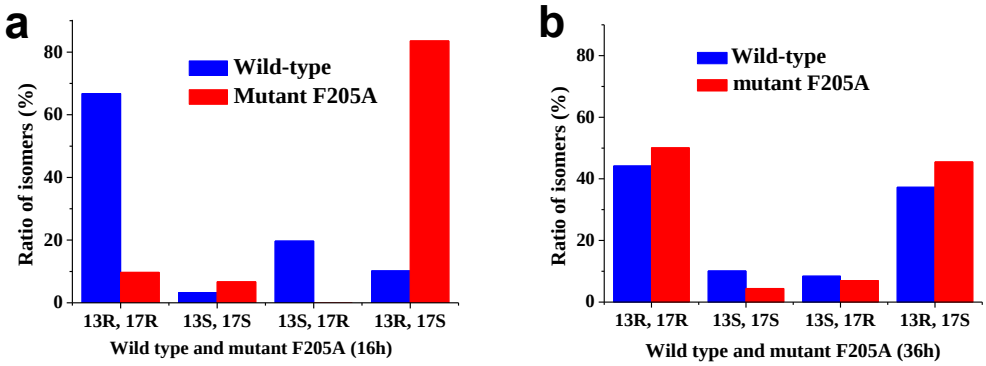

Supplementary Fig. 1. Stereoselectivity variation during biotransformation. a, Stereoselectivity of wild-type enzyme and mutant F205A at the reaction time of 16 hours. **b**, Stereoselectivity of wild-type enzyme and mutant F205A at the reaction time of 36 hours.

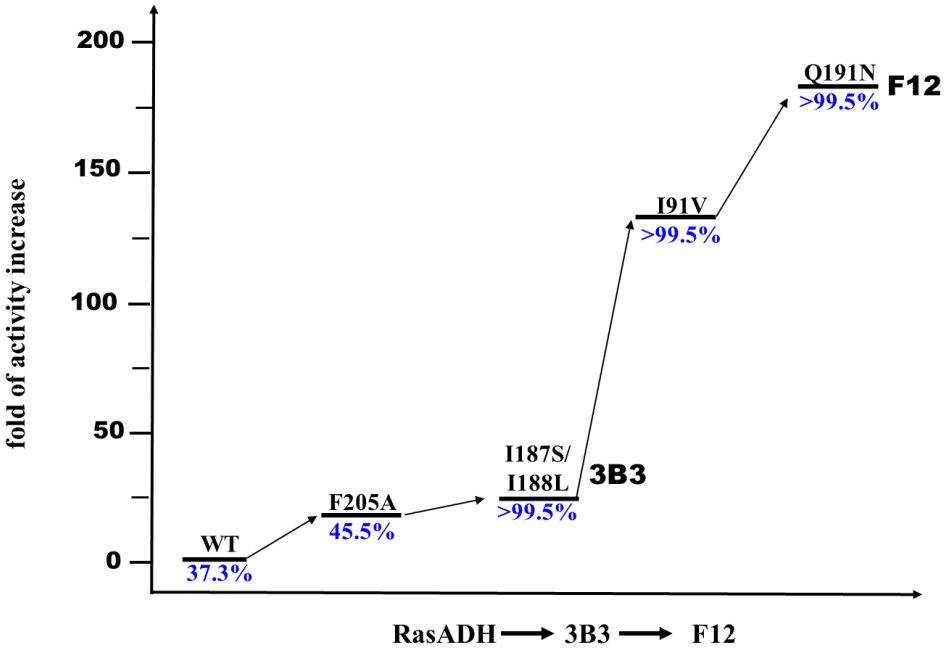

Supplementary Fig. 2. The iterative stepwise improvement process of directed evolution of RasADH. Enzyme activity of WT is taken as 1.0. The percentage of (13*R*, 17*S*)-**2a** among the ketol product of redution are shown in blue.

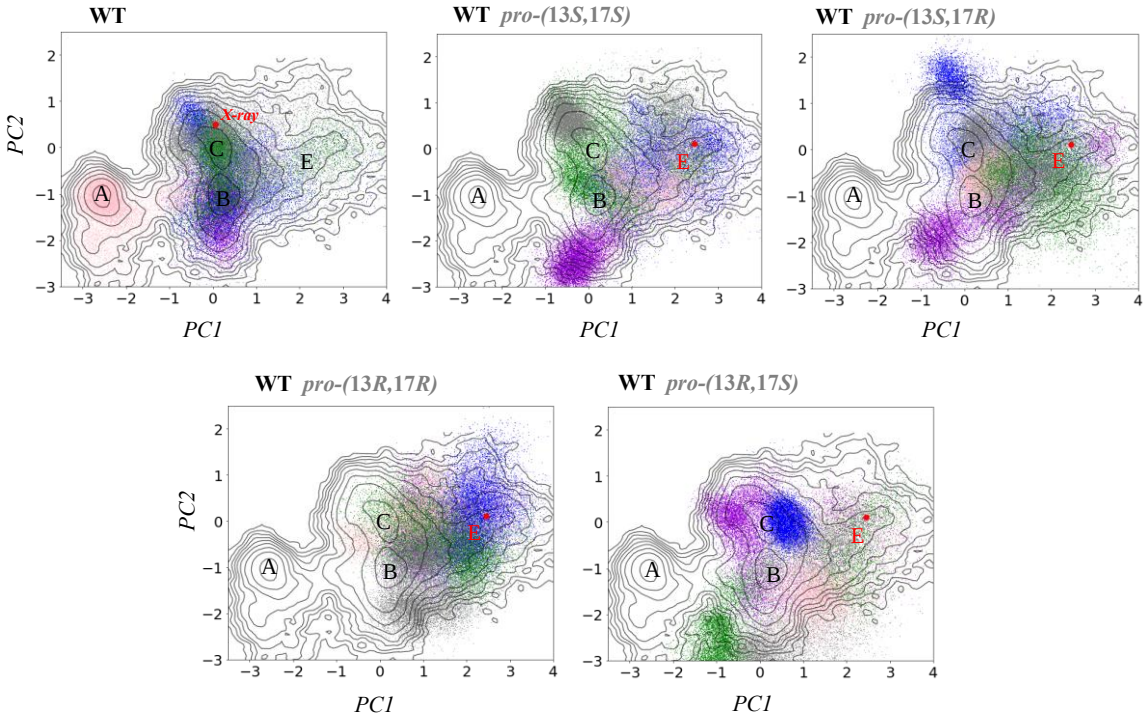

Supplementary Fig. 3. **Projection of the WT five independent 250 ns MD simulation replicas.** They are represented with small colored dots in either violet (replica 1), blue (rep 2), pink (rep 3), green (rep 4), or gray (rep 5) on the FEL associated with the two most important principal components (PC1, PC2) for RasADH WT. All replicas in the absence of substrate started from the X-ray structure (PDB ID: 4BMS, see red dot in WT figure). For the substrate-bound MD simulations, the starting conformation was the open state (WT-E, marked with a red dot) for the *pro*-(13*S*,17*S*), *pro*-(13*S*,17*R*), *pro*-(13*R*,17*R*) and pro-(13*R*,17*S*) orientations.

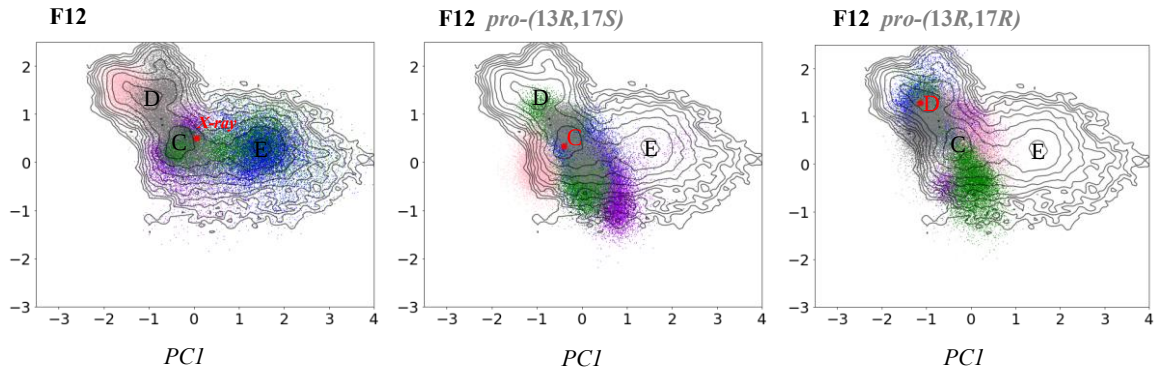

Supplementary Fig. 4. **Projection of the F12 five independent 250 ns MD simulation replicas**. They are represented with small colored dots in either violet (replica 1), blue (rep 2), pink (rep 3), green (rep 4), or gray (rep 5) on the FEL associated with the two most important principal components (PC1, PC2) for F12 enzyme variant. All replicas in the absence of substrate started from the X-ray structure (PDB ID: 4BMS, see red dot in F12 figure). For the substrate-bound MD simulations, the starting conformation was the partially closed states (F12-C) and (F12-D) for the *pro*-(13*R*,17*S*) and the *pro*-(13*R*,17*R*) orientations, respectively.

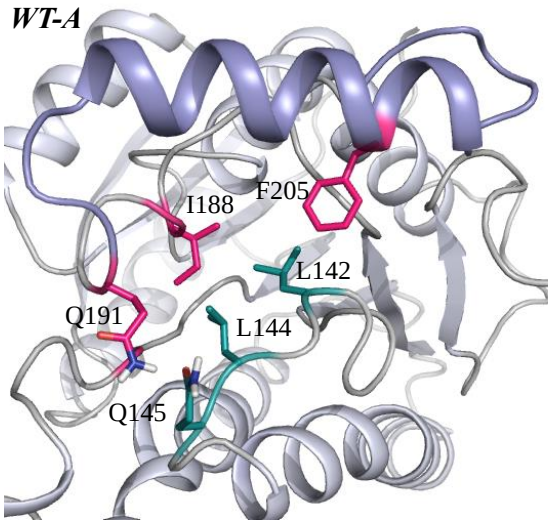

Supplementary Fig. 5. Representation of the WT-A conformation. As it is shown, the Q191, I188 and F205 subjected to mutagenesis (shown in pink) perform non-covalent interactions with Q145, L144 and L142 active site loop residues (in teal) stabilizing the closed state. The NADPH cofactor is not shown for clarity.

Note: The closed state sampled in WT-A is stabilised by the formation of non-covalent interactions occurring between positions F205, I188 and Q191 and residues L142, L144 and Q145 of an active site loop. It is interesting to remark that some of these residues are mutated in F12 variant (F205A, I188L and Q191N), which explains the absence of closed states (F12-A) in the case of the evolved enzyme.

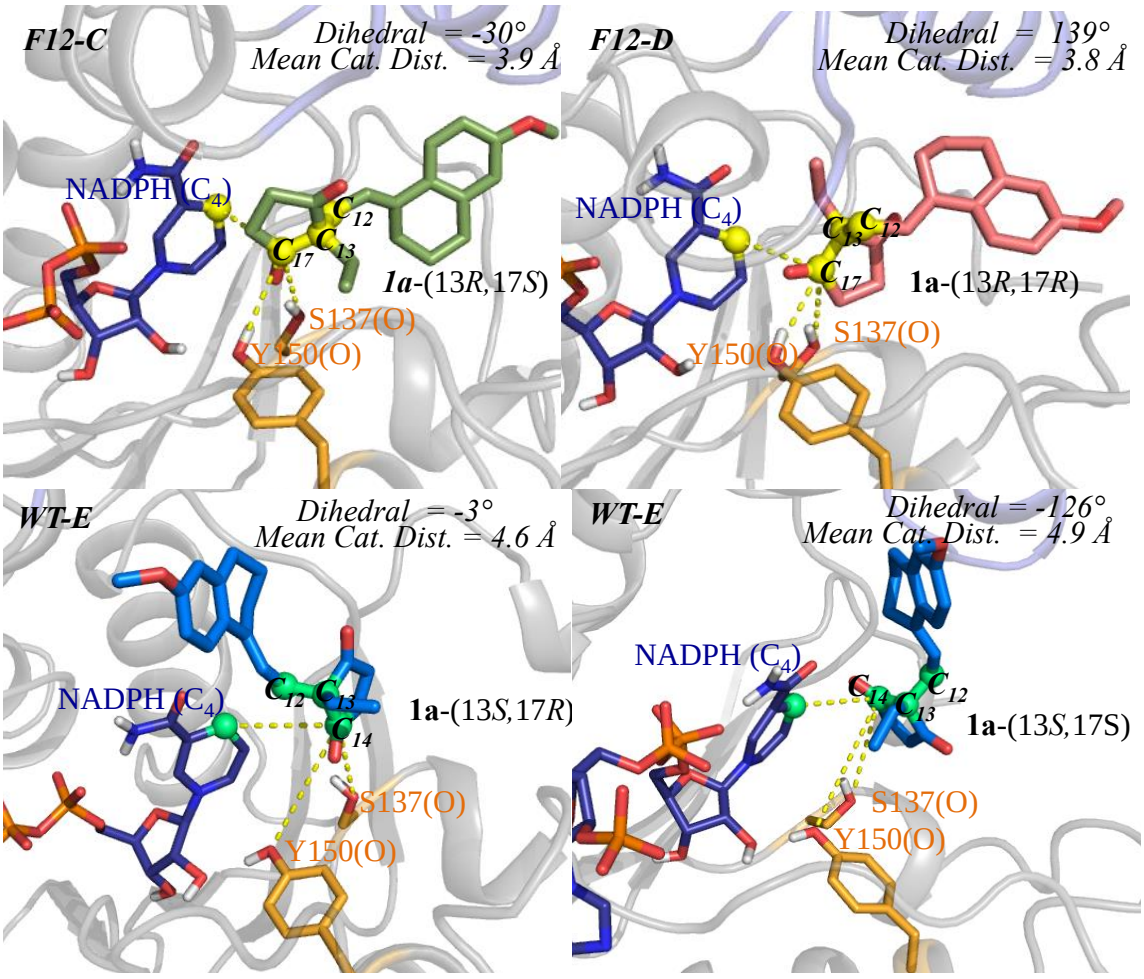

Supplementary Fig. 6. Representation of the selected atoms for dihedral calculation. NADPH (C_4), **1a**($C_{17/14}$), **1a**(C_{13}) and **1a**(C_{12}) are in spheres together with the catalytic distances: hydride transfer NADPH (C4N)-**1a**($C_{17/14}$)) and proton donor (S137(O)-**1a**($C_{17/14}$) and Y150(O)-**1a**($C_{17/14}$)) distances represented in dashed lines. Note that dihedrals and distances with **1a**(C_{17}) measures the pro-(13*R*,17*S*)/(13*R*,17*R*) orientations, while **1a** (C_{14}) pro-(13*S*,17*S*)/(13*S*,17*R*). The dihedral angle shown was selected to distinguish the 4 possible stereopreferences of **1a** obtained by docking predictions. Dihedral angles leading to *pro-(*13*R*,17*S*) orientations of the substrate lie between -60 and 0º, between 110 and 170º for *pro*-(13*R*,17*R*), between -170 and -110º for *pro*-(13*S*,17*S*) and between -30 and 30º for *pro*-(13*S*,17*R*).

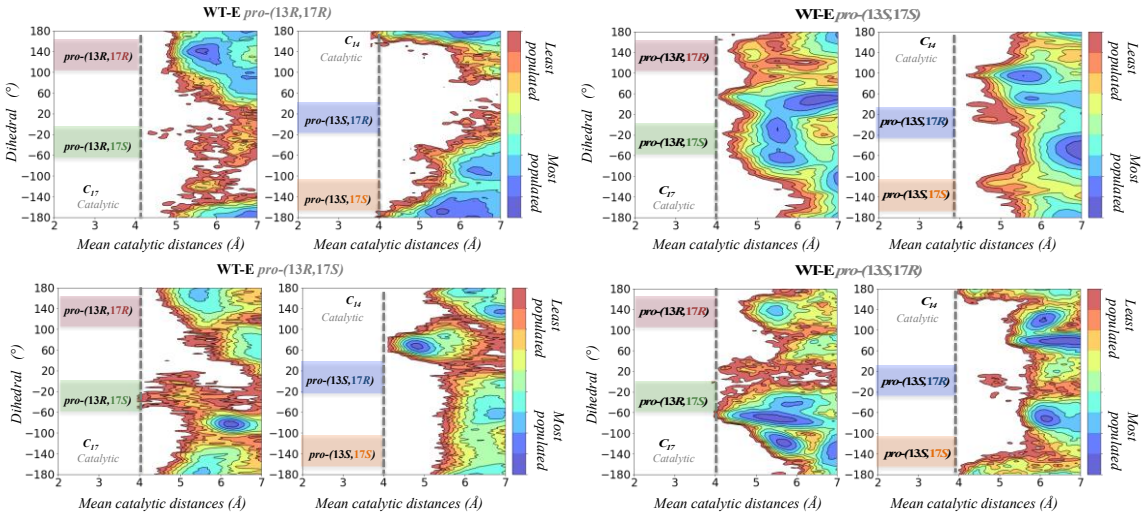

Supplementary Fig. 7. Conformational population analysis of WT-E. Conformational population analysis associated with the dihedral and the mean catalytic distances (detailed in Supplementary Fig. 5) sampled along the MD simulations for the WT-E starting from the *pro*-(13*R*,17*R*), *pro*-(13*R*,17*R*), *pro*-(13*S*,17*S*) and *pro*-(13*S*,17*R*) orientations. Dihedral angles leading to *pro-(*13*R*,17*S*) orientations of the substrate lie between -60 and 0º (highlighted with a green area), between 110 and 170º for *pro*-(13*R*,17*R*) (represented in red), between -170 and -110º for *pro*-(13*S*,17*S*) (represented in orange) and between -30 and 30º for *pro*-(13*S*,17*R*) (represented in blue).

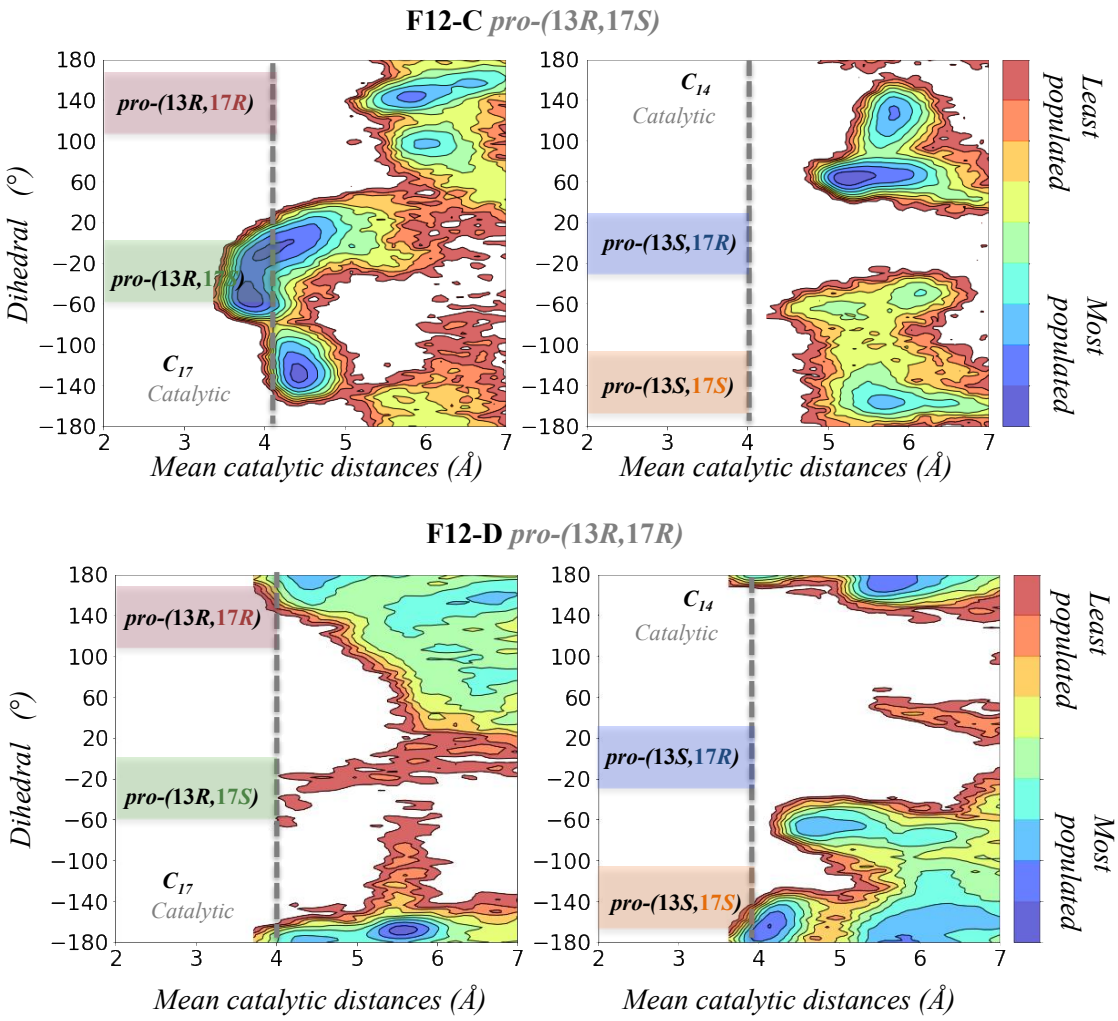

Supplementary Fig. 8. Conformational population analysis of F12-C and F12-D. Conformational population analysis associated with the dihedral and the mean catalytic distances (detailed in Supplementary Fig. 6) sampled along the MD simulations for F12-C and F12-D starting from the *pro*-(13*R*,17*S*) and the *pro*-(13*R*,17*R*) orientations, respectively. Dihedral angles leading to *pro*-(13*R*,17*S*) orientations of the substrate lie between -60 and 0º (highlighted with a green area), between 110 and 170º for *pro*-(13*R*,17*R*) (represented in red), between -170 and 110º for *pro*-(13*S*,17*S*) (represented in orange) and between -30 and 30º for *pro*-(13*S*,17*R*) (represented in blue).

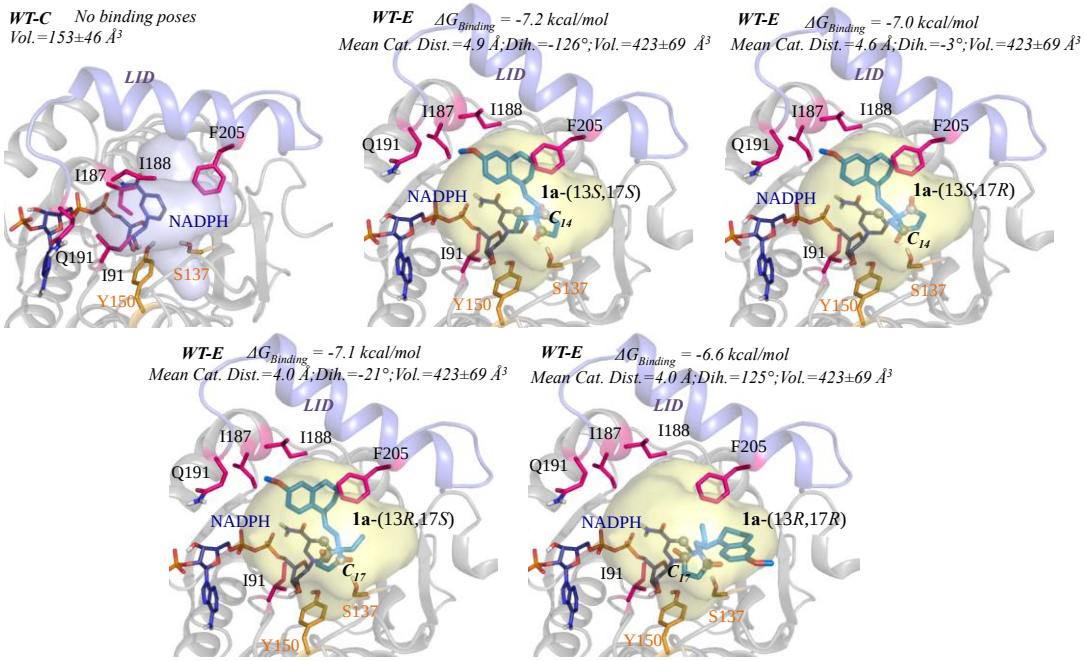

Supplementary Fig. 9. Detailed representation of the active site of WT-C and WT-D meta-stable conformations. The active site is bound with **1a**, the computed volumes, respective dihedrals and catalytic distances are also shown.

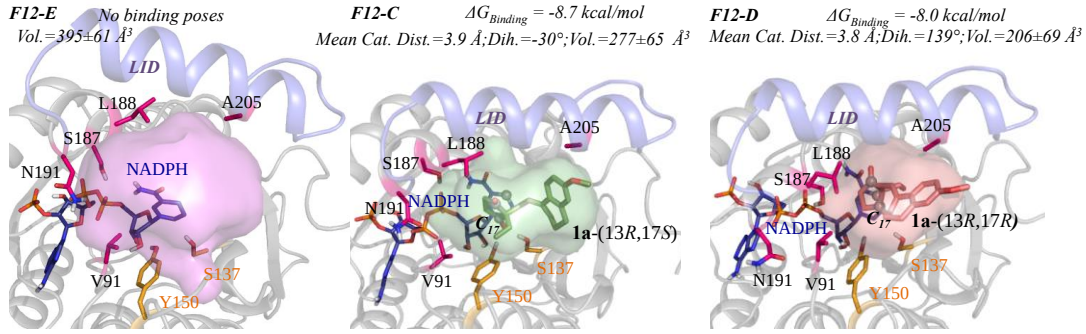

Supplementary Fig. 10. Detailed representation of the active site of F12-C, F12-D, and F12-E meta-stable conformations. The active site is bound with **1a**, the computed volumes, respective dihedrals and catalytic distances are also shown.

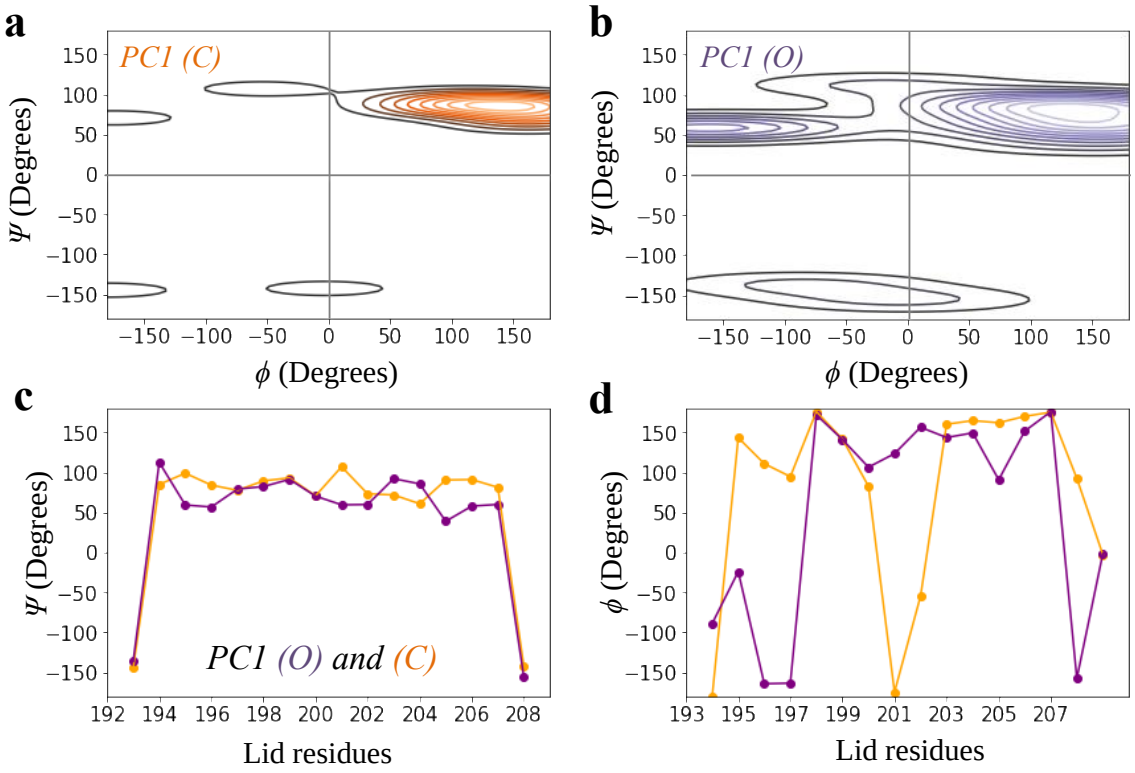

Supplementary Fig. 11. Representation of the Ramachandran plot of the lid region. The Ramachandran plots of the lid region (α6 helix, residues 194-209) for the closed (C) in orange (a) and the open (O) in purple (b) conformations associated to the most important principal component (PC1) are presented. The psi(Ψ) and phi(ϕ) dihedral values for each residue in the lid (194-209) of the open (O) and closed (C) conformations are shown in (c) and (d). As observed in the plots, the most dramatic changes take place for the phi(ϕ) dihedral angles of residues 195-197, 200-202, and 208.

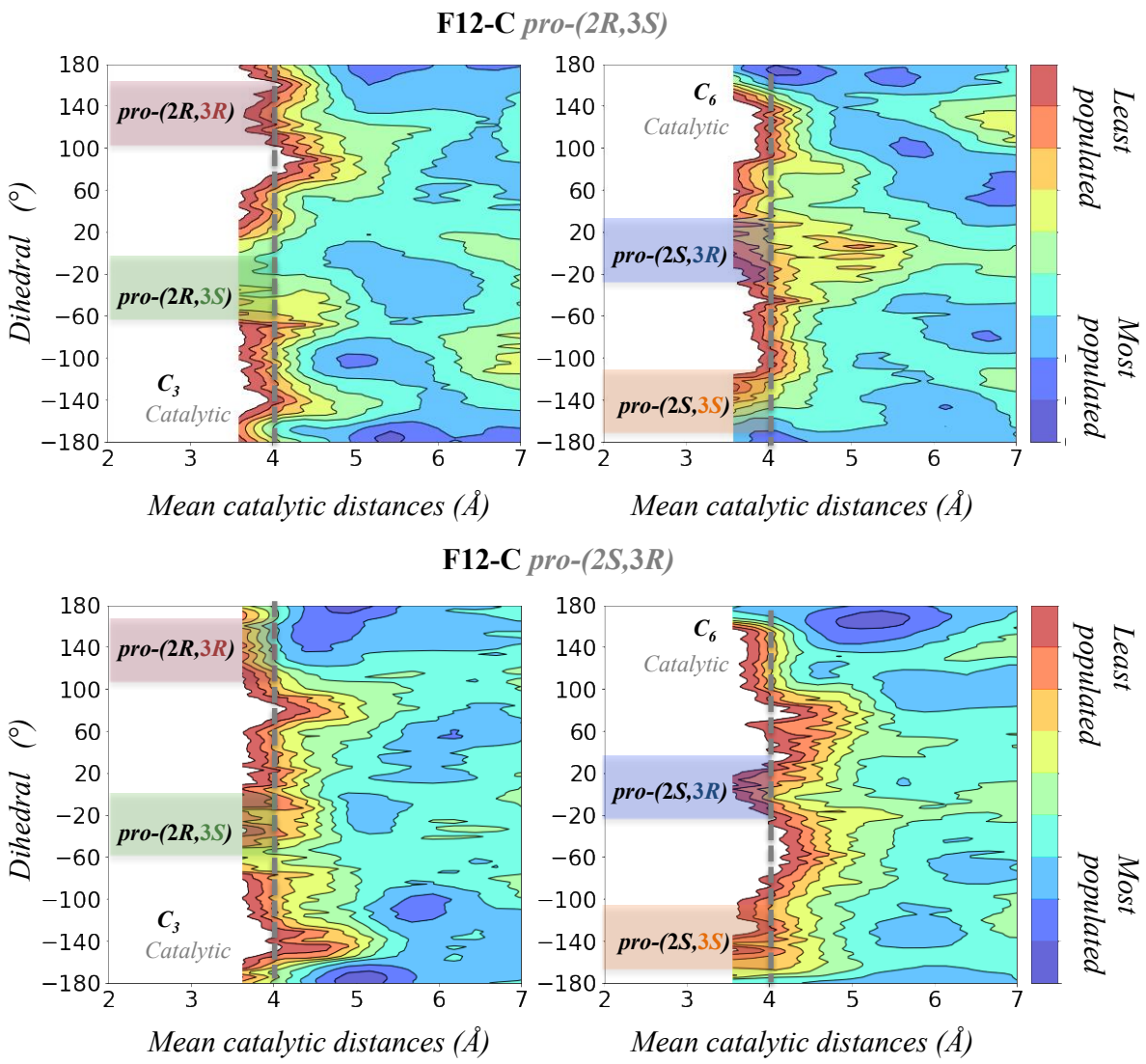

Supplementary Fig. 12. Conformational population analysis of F12 with 3k. Conformational population analysis associated with the dihedral and the mean catalytic distances using **3k** as substrate, and starting the MD simulations from the *pro*-(2*R*, 3*S*) and *pro*-(2*S*, 3*R*) orientations in F12-C. Dihedral angles leading to *pro*-(2*R*, 3*S*) orientations of **3k** lie between -60 and 0º (highlighted with a green area), between 110 and 170º for *pro*-(2*R*, 3*R*) (represented in red), between -170 and -110º for *pro*-(2*S*, 3*S*) (represented in orange) and between -30 and 30º for *pro*-(2*S*, 3*R*) (represented in blue). The lower stereoselectivity and activity observed for **3k** experimentally is consistent its smaller size, as it can adopt many unproductive orientations in the wide F12 active site pocket.

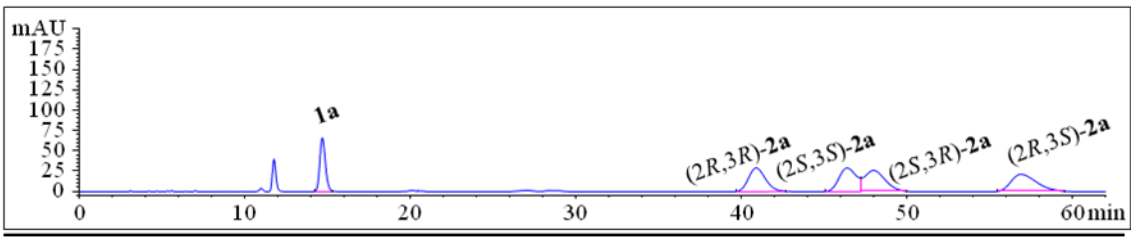

Peak	RT(mins)	Area	Area%
(2*R*,3*R*)-**2a**	40.870	1978.8	23.774
(2*S*,3*S*)-**2a**	46.423	2035.8	24.459
(2*S*,3*R*)-**2a**	48.007	2168.7	26.055
(2*R*,3*S*)-**2a**	56.890	2140.1	25.712

Supplementary Fig. 13. HPLC traces of 1a and $NaBH_4$-reduction products 2a.

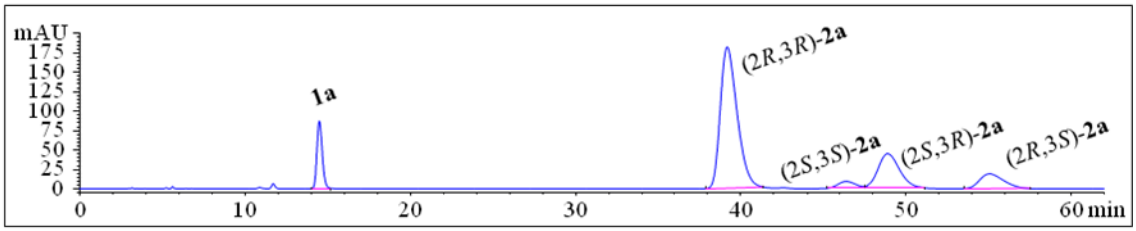

Peak	RT(mins)	Area	Area%
(2*R*,3*R*)-**2a**	39.160	12961.8	66.810
(2*S*,3*S*)-**2a**	46.431	641.4	3.306
(2*S*,3*R*)-**2a**	48.890	3831.6	19.749
(2*R*,3*S*)-**2a**	55.053	1966.3	10.135

Supplementary Fig. 14. HPLC traces of the WT enzyme reduction products 2a in 16h.

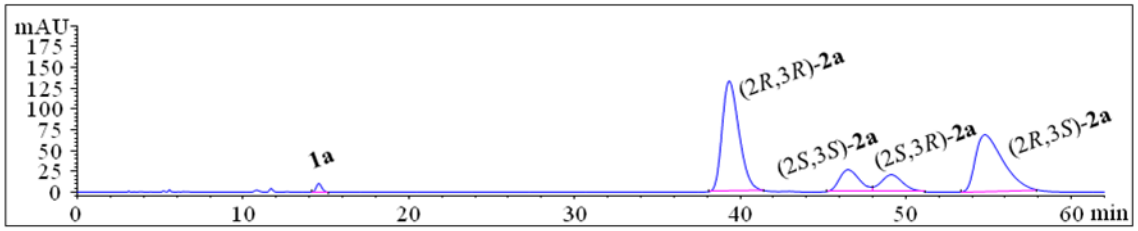

Peak	RT(mins)	Area	Area%
(2*R*,3*R*)-**2a**	39.335	9425.9	44.248
(2*S*,3*S*)-**2a**	46.509	2163.9	10.158
(2*S*,3*R*)-**2a**	49.114	1802.4	8.461
(2*R*,3*S*)-**2a**	54.784	7910.3	37.133

Supplementary Fig. 15. HPLC traces of the WT enzyme reduction products 2a in 36h.

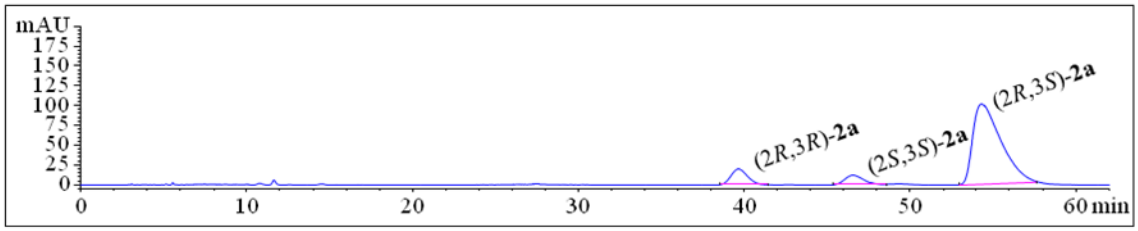

Peak	RT(mins)	Area	Area%
(2*R*,3*R*)-**2a**	39.662	1364.8	9.620
(2*S*,3*S*)-**2a**	46.580	957.2	6.747
(2*R*,3*S*)-**2a**	54.333	11865.3	83.633

Supplementary Fig. 16. HPLC traces of the mutant F205A reduction products 2a in 16h.

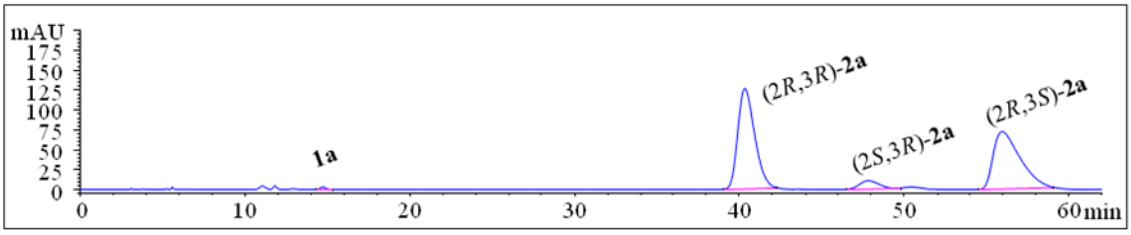

Peak	RT(mins)	Area	Area%
(2*R*,3*R*)-**2a**	40.322	9066.8	50.133
(2*S*,3*R*)-**2a**	47.802	802.9	4.439
(2*R*,3*S*)-**2a**	55.955	8215.7	45.427

Supplementary Fig. 17. HPLC traces of the mutant F205A reduction products 2a in 36h.

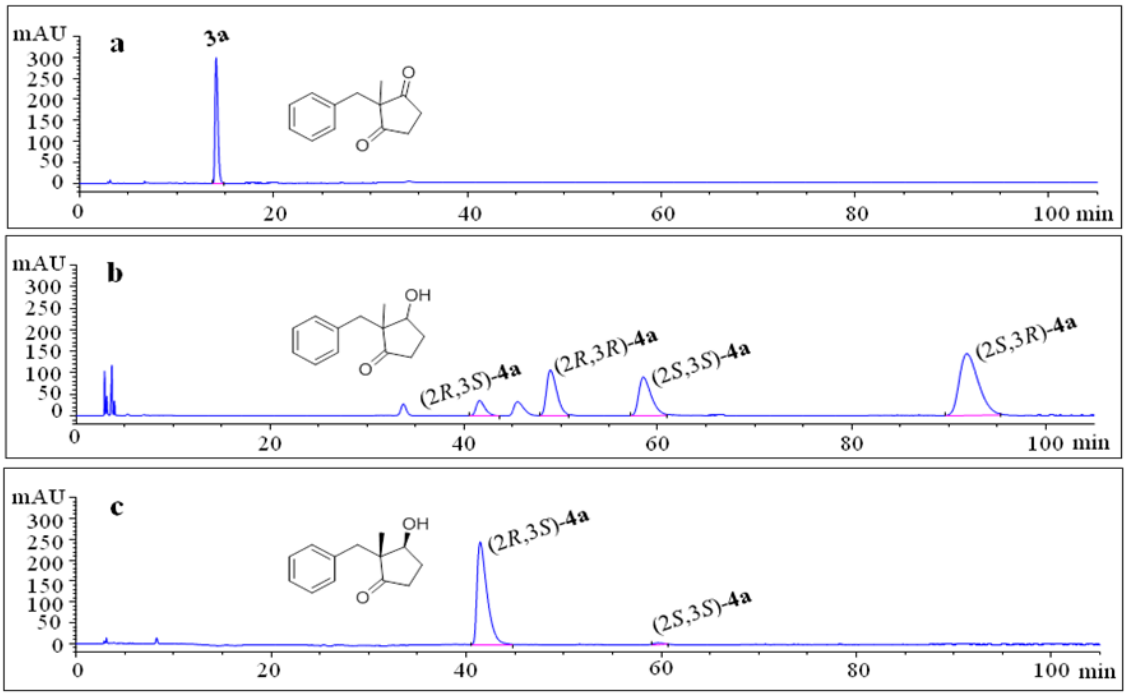

Peak	RT(mins)	Area	Area%
(2*R*,3*S*)-**4a**	41.443	18214.6	98.825
(2*S*,3*S*)-**4a**	59.695	216.6	1.175

Supplementary Fig. 18. HPLC traces for a) the 3a standard, b) the $NaBH_4$-reduction products (racemic diastereomers) 4a and c) the enzymatic reduction products 4a.

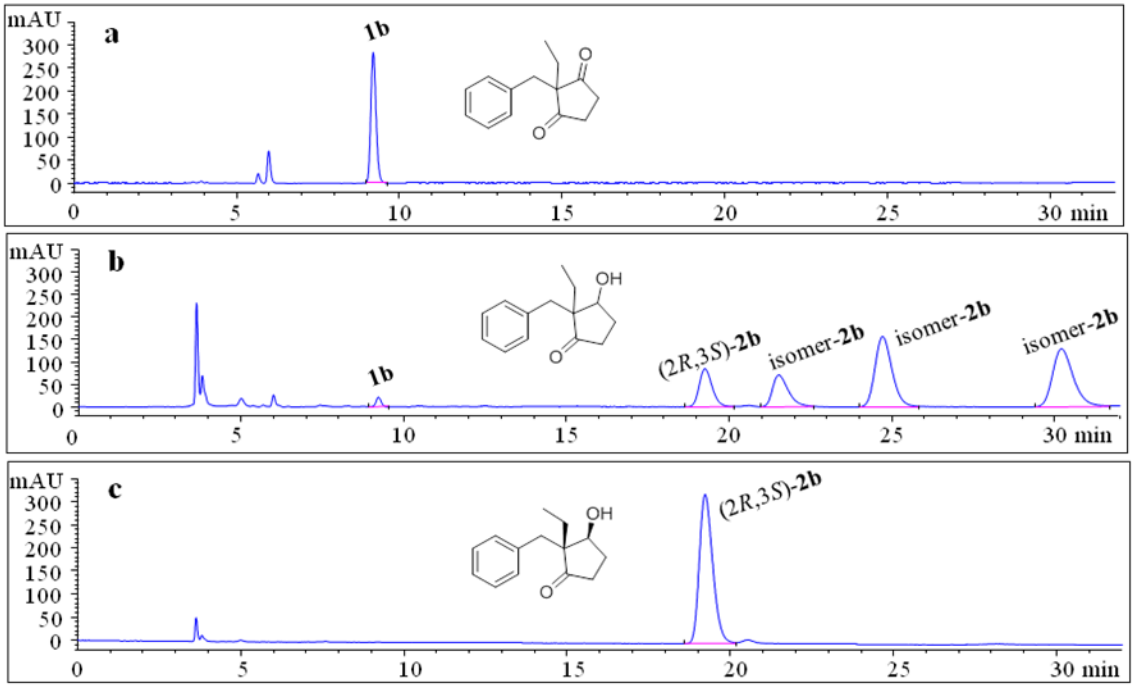

Peak	RT(mins)	Area	Area%
(2*R*,3*S*)-**2b**	19.222	9352.6	100.000

Supplementary Fig. 19. HPLC traces for a) the 1b standard, b) the NaBH$_4$-reduction products (racemic diastereomers) 2b and c) the enzymatic reduction products 2b.

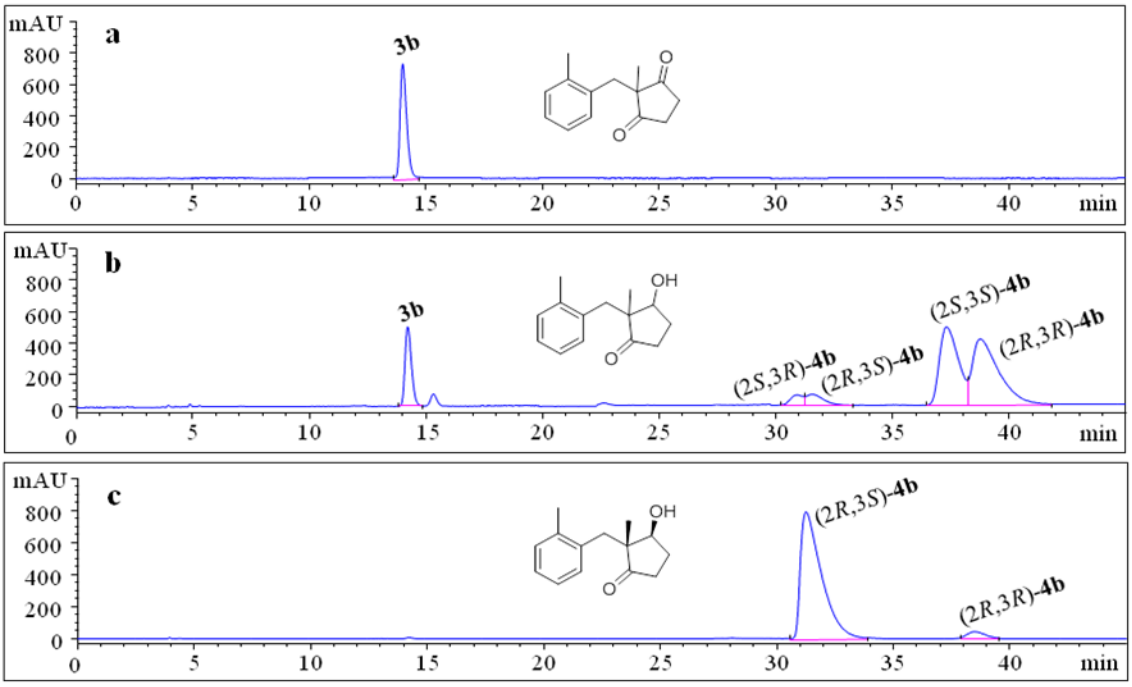

Peak	RT(mins)	Area	Area%
(2*R*,3S)-**4b**	31.242	49231.1	95.496
(2*R*,3*R*)-**4b**	38.523	2322.0	4.504

Supplementary Fig. 20. HPLC traces for a) the 3b standard, b) the $NaBH_4$-reduction products (racemic diastereomers) 4b and c) the enzymatic reduction products 4b.

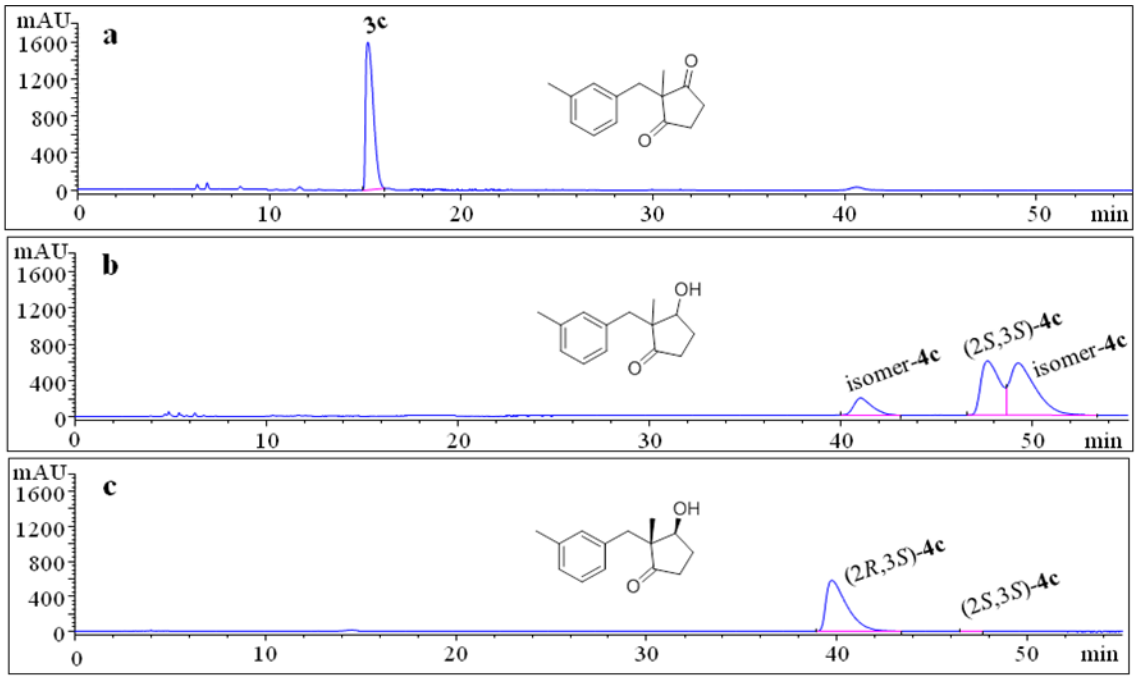

Peak	RT(mins)	Area	Area%
(2*R*,3*S*)-**4c**	39.769	44491.8	99.452
(2*S*,3*S*)-**4c**	46.915	245.3	0.548

Supplementary Fig. 21. HPLC traces for a) the 3c standard, b) the $NaBH_4$-reduction products (racemic diastereomers) 4c and c) the enzymatic reduction products 4c.

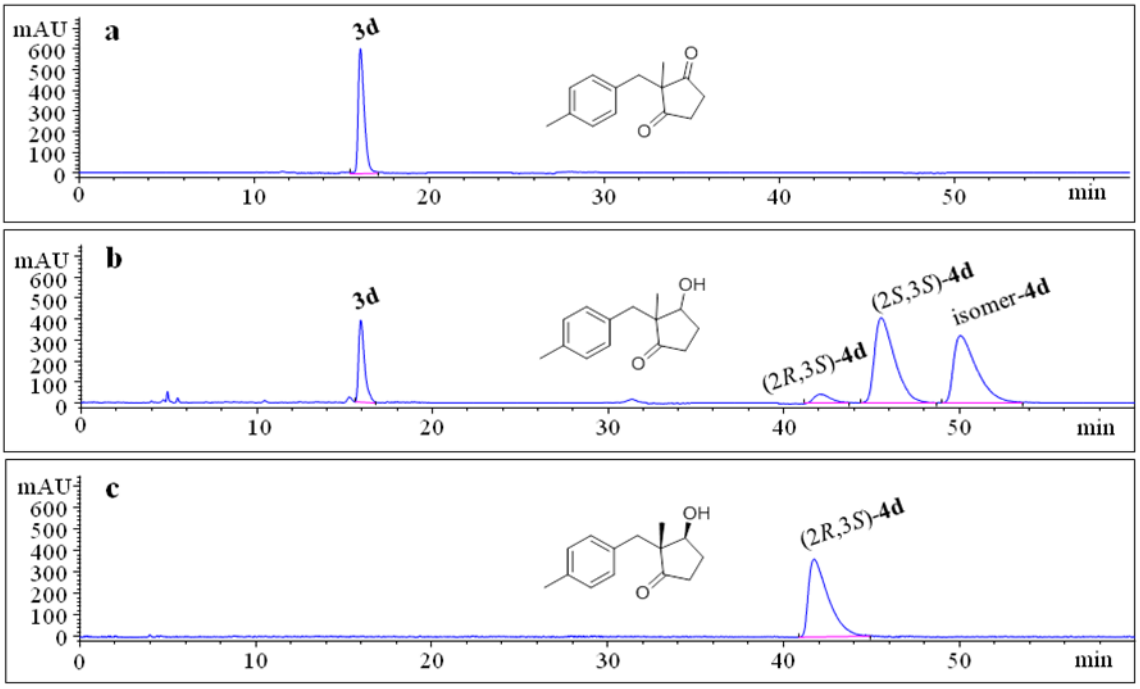

Peak	RT(mins)	Area	Area%
(2*R*,3*S*)-**4d**	41.722	29073.6	100.000

Supplementary Fig. 22. HPLC traces for a) the 3d standard, b) the $NaBH_4$-reduction products (racemic diastereomers) 4d and c) the enzymatic reduction products 4d.

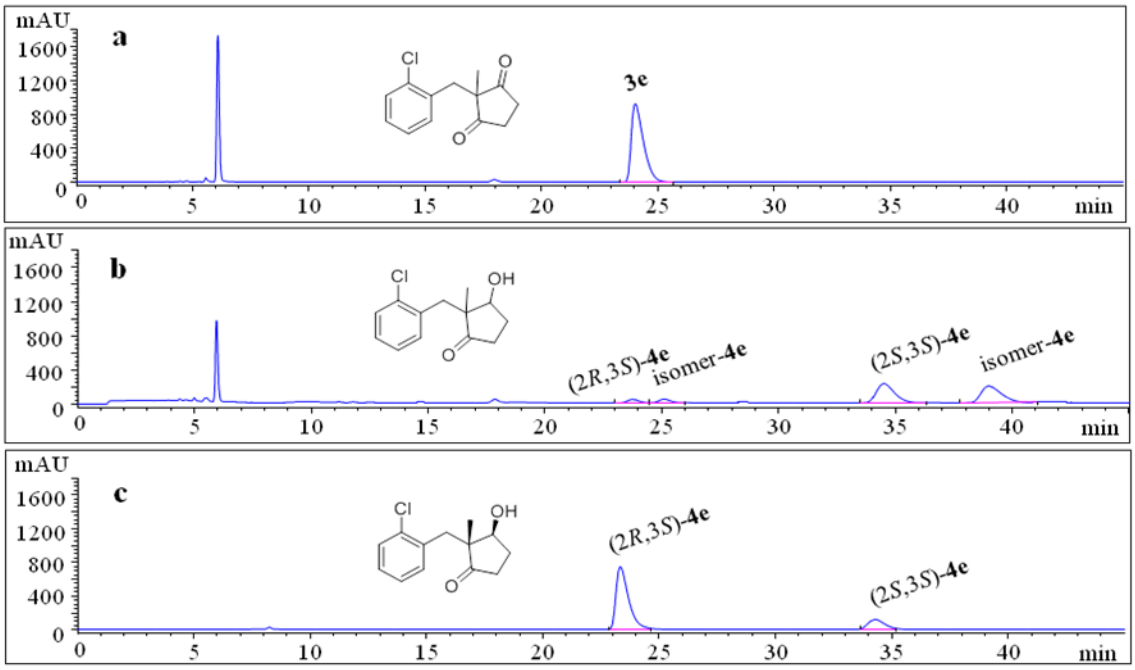

Peak	RT(mins)	Area	Area%
(2*R*,3*S*)-**4e**	23.353	28279.4	83.021
(2*S*,3*S*)-**4e**	34.279	5783.5	16.979

Supplementary Fig. 23. HPLC traces for a) the 3e standard, b) the $NaBH_4$-reduction products (racemic diastereomers) 4e and c) the enzymatic reduction products 4e.

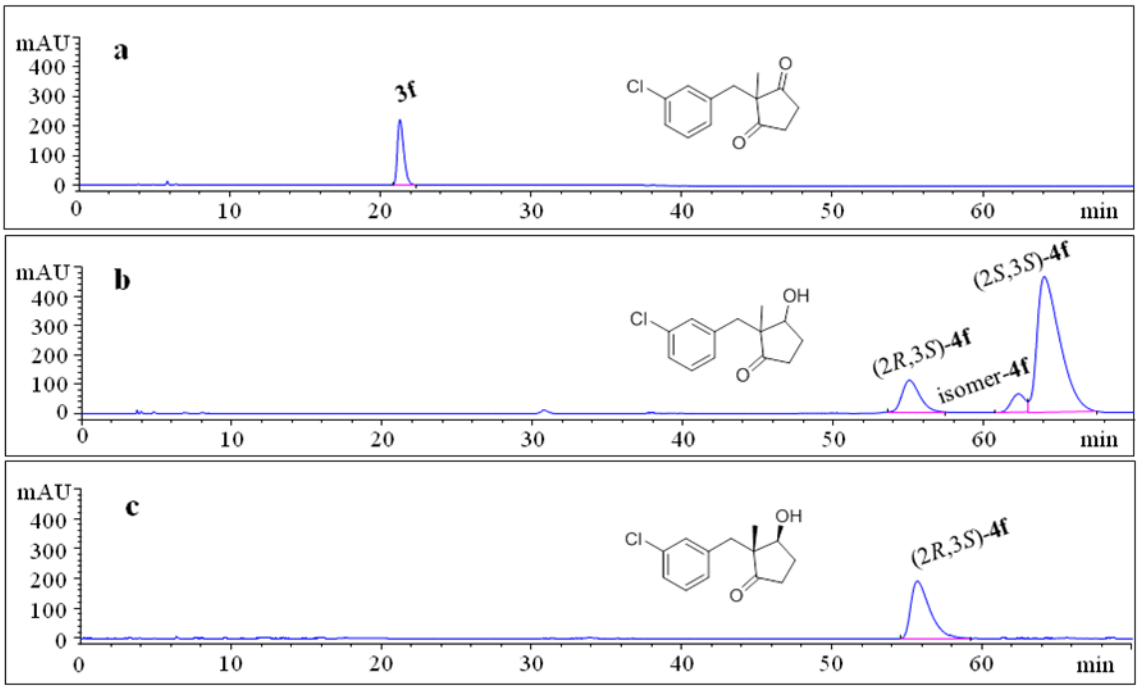

Peak	RT(mins)	Area	Area%
(2*R*,3*S*)-**4f**	55.707	16618.1	100.000

Supplementary Fig. 24. HPLC traces for a) the 3f standard, b) the $NaBH_4$-reduction products (racemic diastereomers) 4f and c) the enzymatic reduction products 4f.

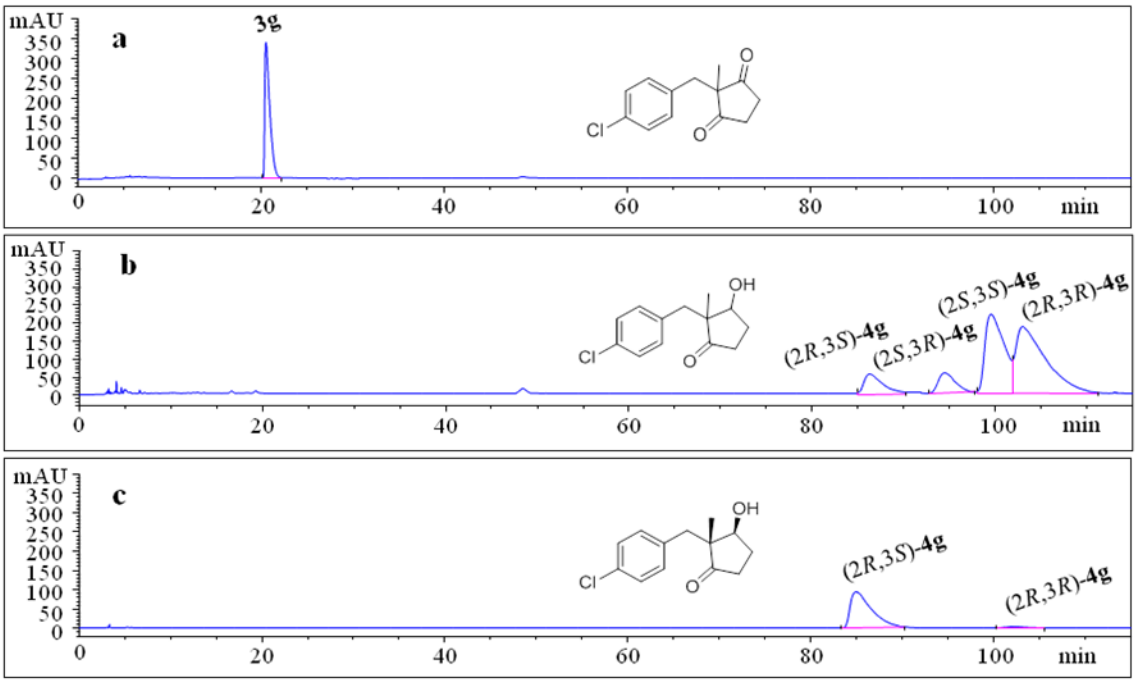

Peak	RT(mins)	Area	Area%
(2*R*,3*S*)-**4g**	84.911	15538.0	95.139
(2*R*,3*R*)-**4g**	101.894	793.9	4.861

Supplementary Fig. 25. HPLC traces for a) the 3g standard, b) the $NaBH_4$-reduction products (racemic diastereomers) 4g and c) the enzymatic reduction products 4g.

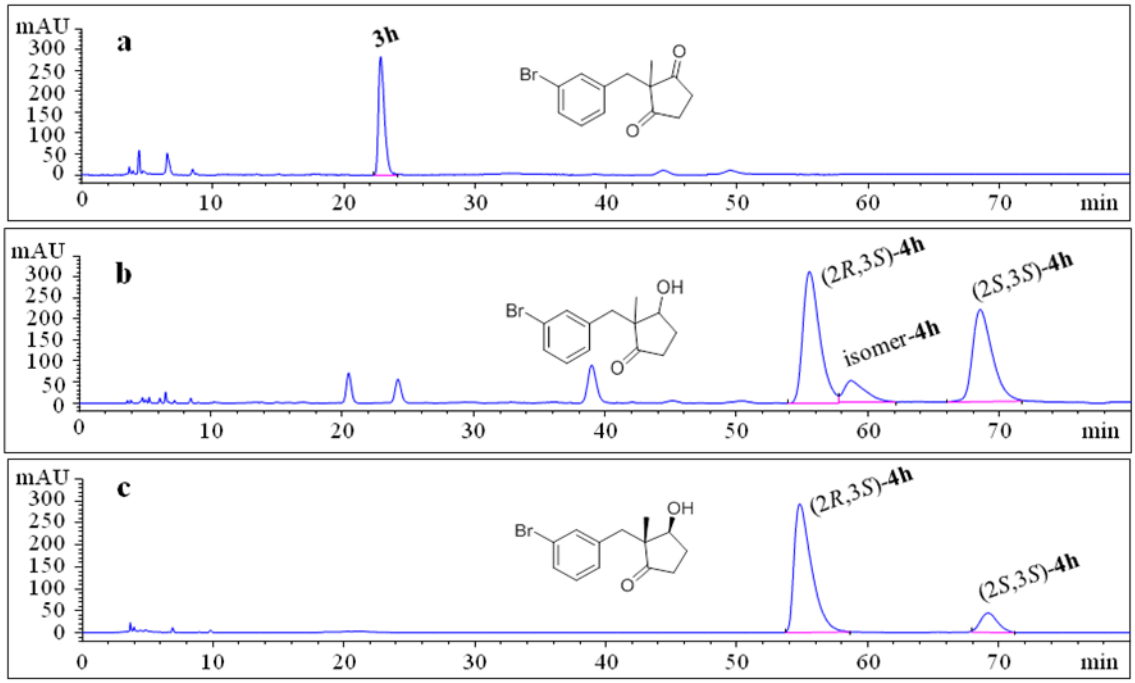

Peak	RT(mins)	Area	Area%
(2*R*,3*S*)-**4h**	54.828	27408.6	86.469
(2*S*,3*S*)-**4h**	69.186	4289.2	13.531

Supplementary Fig. 26. HPLC traces for a) the 3h standard, b) the $NaBH_4$-reduction products (racemic diastereomers) 4h and c) the enzymatic reduction products 4h.

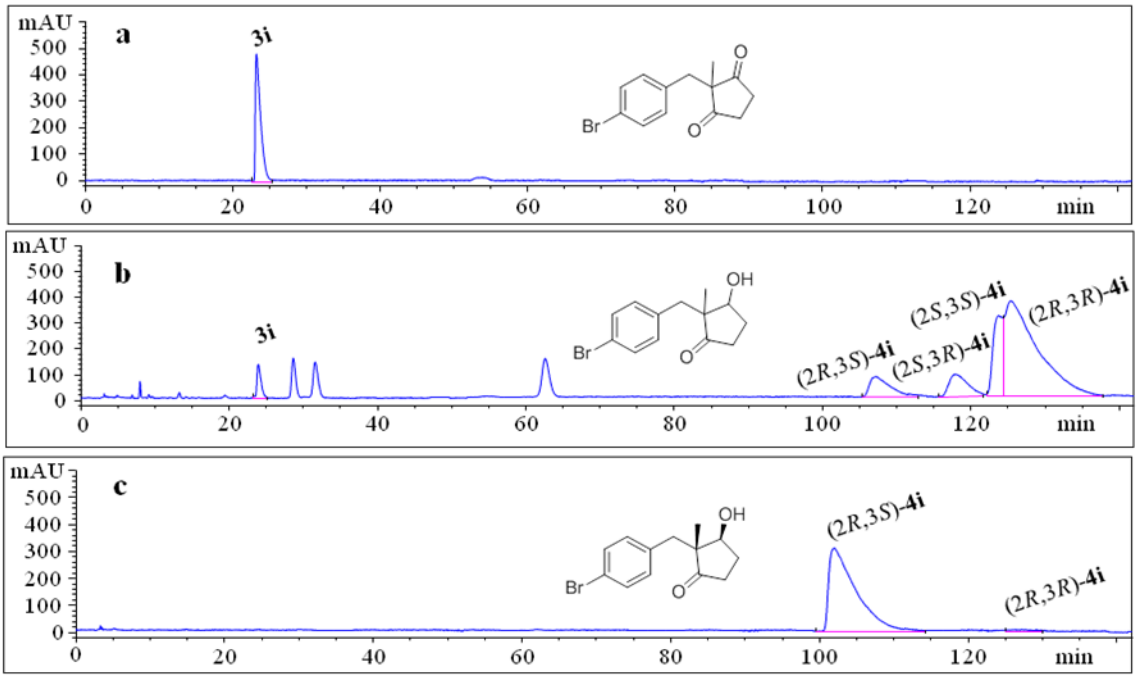

Peak	RT(mins)	Area	Area%
(2*R*,3*S*)-**4i**	101.884	78229.1	98.727
(2*R*,3*R*)-**4i**	127.178	1009.0	1.273

Supplementary Fig. 27. HPLC traces for a) the 3i standard, b) the $NaBH_4$-reduction products (racemic diastereomers) 4i and c) the enzymatic reduction products 4i.

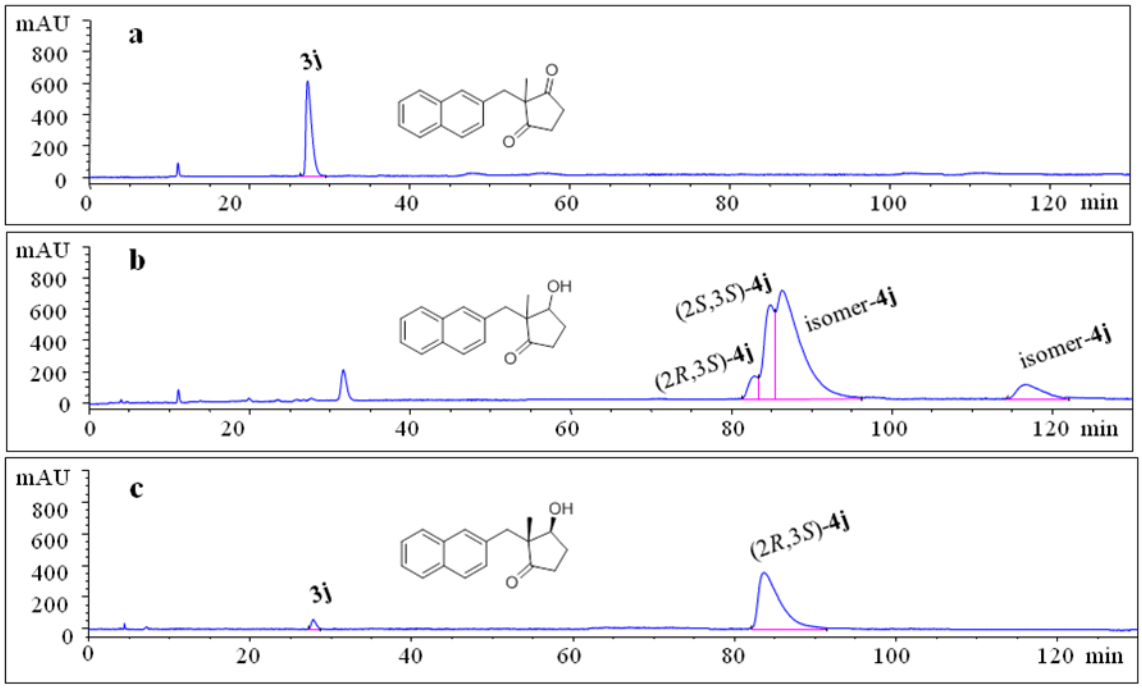

Peak	RT(mins)	Area	Area%
(2*R*,3*S*)-**4j**	83.604	64514.7	100.000

Supplementary Fig. 28. HPLC traces for a) the 3j standard, b) the NaBH$_4$-reduction products (racemic diastereomers) 4j and c) the enzymatic reduction products 4j.

Supplementary References

1. Brooks, D. W., Mazdiyasni H & Grothaust P. G. Asymmetric microbial reduction of prochiral 2,2-disubstituted cycloalkanediones. *J. Org. Chem.* **52**, 3232-3239 (1987).

2. Contente, M. L. et al, Stereoselective reduction of aromatic ketones by a new ketoreductase from *Pichia glucozyma*. *Appl. Microbiol. Biotechnol.* **100**, 193-201 (2016).

3. Rocco, R. et al. A novel archaebaterial NAD$^+$-dependent alcohol dehydrogenase purification and properties. *Eur. J. Biochem.* **167**, 475-479 (1987).

4. Liu, Y. et al Regio- and stereoselective reduction of 17-oxosteroids to 17beta-hydroxysteroids by a yeast strain Zygowilliopsis sp. WY7905. *Steroids* **118**, 17-24 (2017).

5. Yang, Y., Zhu, D., Piegat, T. J. & Hua, L. Enzymatic ketone reduction: mapping the substrate profile of a short-chain alcohol dehydrogenase (YMR226c) from *Saccharomyces*

cerevisiae. *Tetrahedron: Asymmetry* **18**, 1799-1803 (2007).

6. Peretz, M. et al. Molecular cloning, nucleotide sequecing, and expression of genes encoding alcohol dehydrogenase from the thermophile *Thermoanaerobacter brockii* and the mesophile *Clostridium beijerinckii*. *Anaerobe* **3**, 259-270 (1997).

7. Li, Z. et al. Highly enantioselective double reduction of phenylglyoxal to (*R*)-1-phenyl-1,2-ethanediol by one NADPH-dependent yeast carbonyl reductase with a broad substrate profile. *Tetrahedron* **69**, 3561-3564 (2013).

8. Ema, T., Yagasaki, H., Okita, N., Takeda, M. & Sakai, T. Asymmetric reduction of ketones using recombinant *E. coli* cells that produce a versatile carbonyl reductase with high enantioselectivity and broad substrate specificity. *Tetrahedron* **62**, 6143-6149 (2003).

9. Zhao, F. J., Liu, Y., Pei, X. Q., Guo, C. & Wu, Z. L. Single mutations of ketoreductase ChKRED20 enhance the bioreductive production of (1*S*)-2-chloro-1-(3, 4-difluorophenyl) ethanol. *Appl. Microbiol. Biotechnol.* **101**, 1945-1952 (2017).

10. Zhu, D., Malik, H. T. & Hua, L. Asymmetric ketone reduction by a hyperthermophilic alcohol dehydrogenase. The substrate specificity, enantioselectivity and tolerance of organic solvents. *Tetrahedron: Asymmetry* **17***,* 3010-3014 (2006).

11. Kaluzna, I. A., Matsuda, T., Sewell, A. K. & Stewart, J. D. Systematic investigation of *Saccharomyces cerevisiae* enzymes catalyzing carbonyl reductions. *J. Am. Chem. Soc.* **126***,* 12827-12832 (2004).

12. Liang, J. et al. Ketoreductase polypeptides and uses thereof. *WO200904298 4A1* 2009.

13. Edegger, K. et al. Biocatalytic deuterium- and hydrogen-transfer using over-expressed ADH-'A': enhanced stereoselectivity and 2H-labeled chiral alcohols. *Chem. Commun.* 2402-2404 (2006).

14. Kita, K. et al. Cloning, overexpression, and mutagenesis of the *Sporobolomyces salmonicolor* Aku4429 Gene encoding a new aldehyde reductase, which catalyzes the stereoselective reduction of ethyl 4-chloro-3-oxobutanoate to ethyl (*S*)-4-chloro-3-hydroxybutanoate *Appl. Environ. Microbiol.* **1999,** *65*, 5207-5211 (1999).

15. Lavandera, I. et al. Stereoselective bioreduction of bulky-bulky ketones by a novel ADH from *Ralstoni*a sp. *J. Org. Chem.* **73**, 6003-6005 (2008).